Vacuum 86 (2012) 1701–1708

Contents lists available at SciVerse ScienceDirect

Vacuum

journal homepage: www.elsevier.com/locate/vacuum

Pressure driven rarefied gas flow through a slit and an orifice

S. Misdanitis*, S. Pantazis [1], D. Valougeorgis

University of Thessaly, Department of Mechanical Engineering, Volos 38334, Greece

ARTICLE INFO

Article history:
Received 30 October 2011
Received in revised form
10 January 2012
Accepted 9 February 2012

Keywords:
Rarefied gas dynamics
Kinetic theory
Vacuum flows
Knudsen number

ABSTRACT

The flow of a monatomic gas through a slit and an orifice due to an arbitrarily large pressure difference is examined on the basis of the nonlinear Bhatnagar–Gross–Krook (BGK) model equation, subject to Maxwell diffuse boundary conditions. The governing kinetic equation is discretized by a second-order control volume scheme in the physical space and the discrete velocity method in the molecular velocity space. The nonlinear fully deterministic algorithm is optimized to reduce the computational effort by introducing memory usage optimization, grid refinement and parallelization in the molecular velocity space. Results for the flow rates and the macroscopic distributions of the flow field are presented in a wide range of the Knudsen number for several pressure ratios. The effect of the various geometric and physical parameters on the flow field is examined. Comparison with previously reported corresponding Direct Simulation Monte Carlo (DSMC) results indicates a very good agreement, which clearly demonstrates the accuracy of the kinetic algorithm and furthermore the reliability of the BGK model for simulating pressure driven flows.

1. Introduction

Non-equilibrium flows may appear in several technological fields including microfluidics, vacuum technology and high altitude aerodynamics. The degree of departure from local equilibrium is characterized by the Knudsen number, which is defined as the ratio of the mean free path over a characteristic macroscopic length of the problem. It is well known that when the Knudsen number is larger than 0.1 the typical Navier–Stokes–Fourier formulation is not valid and alternative mesoscale approaches based on kinetic theory, as described by the Boltzmann equation or reliable kinetic model equations, must be implemented.

Over the years, linearized kinetic equations have been extensively applied with great success to solve internal fully developed gas flow through long channels of various cross sections in the whole range of the Knudsen number [1–3]. The numerical solution is fully deterministic based on the discretization of the physical space by finite difference schemes and of the molecular velocity space by discrete velocity methods. Then, the discretized equations are solved in an iterative manner, while synthetic acceleration algorithms may be applied to accelerate the slow convergence of the iteration map at the slip and hydrodynamic regimes [4]. Overall, reliable results for linear fully developed flows through long channels of any cross section may be obtained with moderate computational effort.

However, when the flow becomes nonlinear, i.e. in the case of fast flows through channels of finite length, including flows through slits and orifices, the computational effort is significantly increased. The incoming distribution functions at the entrance and the exit of the channel are not Maxwellians and therefore adequately large computational domains must be included before and after the channel to properly impose the boundary conditions. It is noted that in fully developed flows through long channels the flow is simulated only in one cross section of the channel and then, using a standard methodology [1,2], the mass flow rate is estimated, while in short channels kinetic modeling is required in the whole flow field. This is the main reason for the large computational effort required in the latter case, compared to the one for fully developed flows. The most common approach for solving nonlinear flows is the DSMC method [5], which is a powerful stochastic method for high speed flows, circumventing the solution of a kinetic equation. The DSMC method has been recently implemented to solve flow through slits, orifices and short tubes [6–10]. However, in general this method is associated with large computational effort, certain difficulties in the parallelization of the code and statistical noise for low speed flows. Therefore, it is important to develop alternative approaches based on computationally efficient deterministic solutions of model kinetic equations. Several

* Corresponding author.
E-mail address: semisdan@mie.uth.gr (S. Misdanitis).
[1] Current address: Physikalisch-Technische Bundesanstalt, Berlin 10587, Germany.

0042-207X/$ – see front matter © 2012 Elsevier Ltd. All rights reserved.
doi:10.1016/j.vacuum.2012.02.014

researchers have developed such algorithms [11–13]. However, additional research work in this field is needed.

In the present work, the gas flow through a slit and an orifice has been simulated by introducing a computationally efficient nonlinear fully deterministic algorithm based on the nonlinear BGK kinetic model equation subject to Maxwell diffuse boundary conditions. The kinetic equations have been solved by applying in the physical space a second-order control volume scheme and in the molecular velocity space the discrete velocity method. Gradual grid refinement has been introduced to speed-up the slow convergence of the iterative map in the slip and hydrodynamic regimes [14,15]. Moreover, the code is parallelized in the molecular velocity space, while memory demands are reduced by proper handling of the allocated arrays. Results for the flow rates and the macroscopic quantities are presented in the whole range of the rarefaction for several values of the pressure ratio between the two reservoirs. Comparison with previously reported corresponding DSMC results indicates very good agreement.

2. Flow configuration and computational domain

The flow of a monatomic gas through a slit of height H and through an orifice of radius R contained in an infinitely thin partition that separates two containers is considered. The gas in the containers far from the opening is in equilibrium at pressures P_1 and P_2, with $P_1 > P_2$, and temperatures T_0, which is also the temperature of the partition. The implemented coordinate system is Cartesian for the slit flow and Cylindrical for the orifice flow. Both flow configurations are two-dimensional in the physical space, with the $\hat{x}$ axis denoting the flow direction, while the slit and the orifice are located at $\hat{x} = 0$. The second axis is denoted by $\hat{y}$ in the slit flow and by $\hat{r}$ in the orifice flow. The computational domain consists of the two large computational areas, before and after the partition, defined by $(-X_L \le \hat{x} \le 0, 0 \le \hat{y}, \hat{r} \le Y_L)$ and $(0 \le \hat{x} \le X_R, 0 \le \hat{y}, \hat{r} \le Y_R)$, which correspond to the upstream and downstream reservoirs respectively including the infinitely thin partition which contains the slit $(0 \le \hat{y} \le H/2)$ or the orifice $(0 \le \hat{r} \le R)$. The flow configuration and the computational domain are shown in Fig. 1.

The reference quantities are H, R, T_0, P_1. In addition, N_1 is the reference number density defined as $P_1 = N_1 k_B T_0$, with k_B denoting the Boltzmann constant, while the most probable molecular velocity, defined as $\upsilon_0 = \sqrt{2k_B T_0/m}$ with m denoting the molecular mass, is the reference velocity. The flow is characterized by the reference rarefaction parameter for the slit and the orifice respectively defined as

$$\delta_0^{\text{slit}} = \frac{P_1 H}{\mu_0 \upsilon_0} \quad \textit{and} \quad \delta_0^{\text{orifice}} = \frac{P_1 R}{\mu_0 \upsilon_0} \tag{1}$$

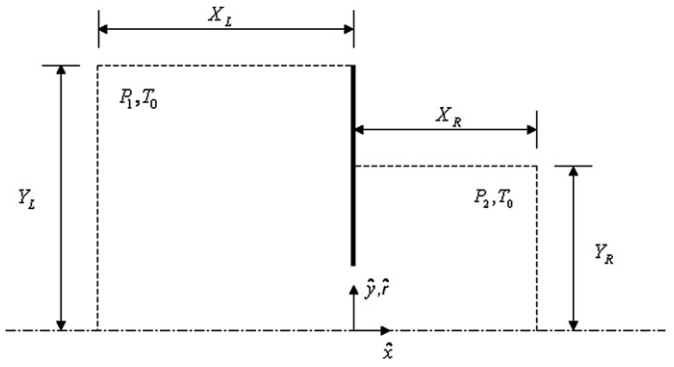

Fig. 1. Upper half of flow configuration and computational domain.

where μ_0 is the gas viscosity at reference temperature T_0. The reference rarefaction is proportional to the inverse of the reference Knudsen number. The objective is to estimate for each flow the flow rates and all macroscopic distributions.

3. Formulation

The flow is modeled by the nonlinear BGK model equation subject to purely diffuse boundary conditions. The choice of the BGK model for simulating the flow is justified by the fact that this is a pressure driven flow and the expected variation of temperature in the flow field is small. The main unknown is the distribution function $f = f(\mathbf{s}, \boldsymbol{\xi})$, while $\mathbf{s} = (\hat{x}, \hat{y})$ or $\mathbf{s} = (\hat{x}, \hat{r})$ is the position vector and $\boldsymbol{\xi} = (\xi_x, \xi_y, \xi_z)$ is the molecular velocity vector. It is seen that the distribution function depends on five independent variables. The local pressure and temperature are defined by P and T respectively.

It is convenient to introduce the following non-dimensional quantities:

$$x = \frac{\hat{x}}{H} \quad \text{or} \quad x = \frac{\hat{x}}{R}, \quad y = \frac{\hat{y}}{H}, \quad r = \frac{\hat{r}}{R}, \quad \boldsymbol{c} = \frac{\boldsymbol{\xi}}{\upsilon_0},$$
$$g = \frac{f\upsilon_0^3}{N_1}, \quad n = \frac{N}{N_1}, \quad \boldsymbol{u} = \frac{\boldsymbol{U}}{\upsilon_0}, \quad \tau = \frac{T}{T_0}, \quad p = \frac{P}{P_1} \tag{2}$$

In subsections 3.1 and 3.2, the formulation of the flow through a slit and an orifice respectively is presented. In both cases, the hard sphere model is implemented and therefore the variation of the viscosity is proportional to the square root of the temperature.

3.1. Flow through a slit

The non-dimensional quantities are introduced into the governing equation to yield [16,17]

$$c_p \cos\theta \frac{\partial g}{\partial x} + c_p \sin\theta \frac{\partial g}{\partial y} = \delta_0 n \sqrt{\tau}\left(g^M - g\right) \tag{3}$$

where $g^M = n/(\pi\tau)^{3/2}\exp[-(\boldsymbol{c}-\boldsymbol{u})^2/\tau]$. Moreover, for computational purposes it is convenient to express the components (c_x, c_y, c_z) of the particle velocity in terms of cylindrical coordinates (c_p, θ, c_z), where $c_p = \sqrt{c_x^2 + c_y^2}$ and $\theta = \tan^{-1}(c_y/c_x)$. Also, by taking advantage of the two-dimensionality of the flow, it is possible to eliminate the c_z component of the distribution function by introducing appropriate projections, expressed by the moments

$$\Phi(x, y, c_x, c_y) = \int_{-\infty}^{\infty} g(x, y, c)\mathrm{d}c_z \quad \text{and}$$
$$\Psi(x, y, c_x, c_y) = \int_{-\infty}^{\infty} c_z^2 g(x, y, c)\mathrm{d}c_z \tag{4}$$

Then, operating accordingly on Eq. (3), after some routine manipulation the following coupled set of integro-differential equations is reduced:

$$c_p \cos\theta \frac{\partial \Phi}{\partial x} + c_p \sin\theta \frac{\partial \Phi}{\partial y} = \delta_0 n \sqrt{\tau}\left(\Phi^M - \Phi\right) \tag{5}$$

$$c_p \cos\theta \frac{\partial \Psi}{\partial x} + c_p \sin\theta \frac{\partial \Psi}{\partial y} = \delta_0 n \sqrt{\tau}\left(\Psi^M - \Psi\right) \tag{6}$$

The corresponding reduced Maxwellians are:

$$\Phi^M = \frac{n}{\pi\tau}\exp\Big[-\Big((c_p\cos\theta-u_x)^2+(c_p\sin\theta-u_y)^2\Big)\Big/\tau\Big] \quad (7)$$

$$\Psi^M = \frac{n}{2\pi}\exp\Big[-\Big((c_p\cos\theta-u_x)^2+(c_p\sin\theta-u_y)^2\Big)\Big/\tau\Big] \quad (8)$$

The macroscopic quantities are expressed in terms of Φ and Ψ as

$$n(x,y) = \int_0^{2\pi}\int_0^{\infty}\Phi c_p\mathrm{d}c_p\mathrm{d}\theta \quad (9)$$

$$u_x(x,y) = \frac{1}{n}\int_0^{2\pi}\int_0^{\infty}(c_p\cos\theta)\Phi c_p\mathrm{d}c_p\mathrm{d}\theta \quad (10)$$

$$u_y(x,y) = \frac{1}{n}\int_0^{2\pi}\int_0^{\infty}(c_p\sin\theta)\Phi c_p\mathrm{d}c_p\mathrm{d}\theta \quad (11)$$

$$\tau(x,y) = \frac{2}{3n}\int_0^{2\pi}\int_0^{\infty}\Big(c_p^2\Phi+\Psi\Big)c_p\mathrm{d}c_p\mathrm{d}\theta-\frac{2}{3}\Big(u_x^2+u_y^2\Big) \quad (12)$$

Based on the above, the slit flow configuration has been reduced to a 4D problem gaining significantly in CPU time without losing any of the physical findings of the flow. The mass flow rate through the slit is calculated by

$$\dot{M}_{\mathrm{slit}} = m\int_{-H/2}^{H/2}N(0,\hat{y})U_x(0,\hat{y})d\hat{y} \quad (13)$$

and is non-dimensionalized by the corresponding mass flow rate for free molecular flow into vacuum $\delta = 0$, $P_2/P_1 = 0$ given by $\dot{M}_{fm,\mathrm{slit}} = (HP_1)/(v_0\sqrt{\pi})$. Then, the dimensionless flow rate is defined as

$$W_{\mathrm{slit}} = \frac{\dot{M}_{\mathrm{slit}}}{\dot{M}_{fm,\mathrm{slit}}} = 4\sqrt{\pi}G_{\mathrm{slit}} \quad (14)$$

where

$$G_{\mathrm{slit}} = \int_0^{1/2}n(0,y)u_x(0,y)dy \quad (15)$$

Turning to the issue of the boundary conditions, it is assumed that molecules are fully accommodated at both sides of the partition and therefore the outgoing distributions are described by Maxwellians having the temperature of the partition. Also, the gas at the fictitious boundaries of the computational domain is assumed in equilibrium and therefore the incoming distributions are approximated by Maxwellians defined by the local pressure P_1 or P_2, temperature T_0 and zero bulk velocity. Symmetry boundary conditions are imposed at $y = 0$. Based on the above, the deduced boundary conditions in dimensionless form for the reduced distributions for the slit flow are:

Upstream reservoir

$$\Phi^+(-X_L/H,y,c_p,\theta) = \Phi^+(x,Y_L/H,c_p,\theta) = \frac{1}{\pi}e^{-c_p^2} \quad (16)$$

$$\Psi^+(-X_L/H,y,c_p,\theta) = \Psi^+(x,Y_L/H,c_p,\theta) = \frac{1}{2\pi}e^{-c_p^2} \quad (17)$$

Downstream reservoir

$$\Phi^+(X_R/H,y,c_p,\theta) = \Phi^+(x,Y_R/H,c_p,\theta) = \frac{P_2}{P_1}\frac{1}{\pi}e^{-c_p^2} \quad (18)$$

$$\Psi^+(X_R/H,y,c_p,\theta) = \Psi^+(x,Y_R/H,c_p,\theta) = \frac{P_2}{P_1}\frac{1}{2\pi}e^{-c_p^2} \quad (19)$$

Partition wall

$$\Phi^+(x\to0^{\mp},y,c_p,\theta) = \frac{\rho_{\mp}^{slit}}{\pi}e^{-c_p^2} \quad (20)$$

$$\Psi^+(x\to0^{\mp},y,c_p,\theta) = \frac{\rho_{\mp}^{slit}}{2\pi}e^{-c_p^2} \quad (21)$$

In all cases the superscripts $(+)$ denotes outgoing distributions, while the notation $(\mp)$ denotes the left $(-)$ and right $(+)$ sides of the partition wall. Finally, in Eqs. (20) and (21) the quantities $\rho_{\mp}$ are specified by the no penetration condition at each side

$$\rho_-^{\mathrm{slit}} = 2\sqrt{\pi}\int_{-\pi/2}^{\pi/2}\int_0^{\infty}(c_p\cos\theta)\Phi\Big(0^-,y,c_p,\theta\Big)c_p\mathrm{d}c_p\mathrm{d}\theta \quad (22)$$

$$\rho_+^{\mathrm{slit}} = -2\sqrt{\pi}\int_{\pi/2}^{3\pi/2}\int_0^{\infty}(c_p\cos\theta)\Phi\Big(0^+,y,c_p,\theta\Big)c_p\mathrm{d}c_p\mathrm{d}\theta \quad (23)$$

3.2. Flow through an orifice

The non-dimensional quantities for the cylindrical geometry are introduced into the governing equation to yield [14,18]

$$c_x\frac{\partial g}{\partial x}+c_p\cos\theta\frac{\partial g}{\partial r}-\frac{c_p\sin\theta}{r}\frac{\partial g}{\partial\theta} = \delta_0 n\sqrt{\tau}\Big(g^M-g\Big) \quad (24)$$

where $g^M = n/(\pi\tau)^{3/2}\exp[-(\boldsymbol{c}-\boldsymbol{u})^2/\tau]$ is the Maxwellian. However, unlike the flow through a slit, the projection procedure can not be implemented in the orifice flow which remains a 5D problem. The macroscopic quantities are given by

$$n(x,r) = 2\int_{-\infty}^{\infty}\int_0^{\pi}\int_0^{\infty}gc_p\mathrm{d}c_p\mathrm{d}\theta\mathrm{d}c_x \quad (25)$$

$$u_x(x,r) = \frac{2}{n}\int_{-\infty}^{\infty}\int_0^{\pi}\int_0^{\infty}c_xgc_p\mathrm{d}c_p\mathrm{d}\theta\mathrm{d}c_x \quad (26)$$

$$u_r(x,r) = \frac{2}{n}\int_{-\infty}^{\infty}\int_0^{\pi}\int_0^{\infty}(c_p\cos\theta)gc_p\mathrm{d}c_p\mathrm{d}\theta\mathrm{d}c_x \quad (27)$$

$$\tau(x,r) = \frac{4}{3n}\int_{-\infty}^{\infty}\int_0^{\pi}\int_0^{\infty}\Big[(c_x-u_x)^2+(c_p\cos\theta-u_r)^2+(c_p\sin\theta)^2\Big]gc_p\mathrm{d}c_p\mathrm{d}\theta\mathrm{d}c_x \quad (28)$$

The mass flow rate through an orifice is calculated by

$$\dot{M}_{\text{orifice}} = 2\pi m \int_0^R N(0,\hat{r}) U_x(0,\hat{r}) \hat{r} d\hat{r} \tag{29}$$

and it is non-dimensionalized by the corresponding mass flow rate for free molecular flow into vacuum $\delta = 0$, $P_2/P_1 = 0$ given by $\dot{M}_{fm,\text{orifice}} = (R^2 P_1 \sqrt{\pi})/(\upsilon_0)$. Then, the dimensionless flow rate is defined as

$$W_{\text{orifice}} = \frac{\dot{M}_{\text{orifice}}}{\dot{M}_{fm,\text{orifice}}} = 4\sqrt{\pi} G_{\text{orifice}} \tag{30}$$

where

$$G_{\text{orifice}} = \int_0^1 n(0,r) u_x(0,r) r dr \tag{31}$$

Next, we move to the description of the boundary conditions regarding the flow through an orifice. Similar assumptions as is the case of the flow through a slit are taken into account. As a result, Maxwellians having the physical characteristics of the partition are the outgoing distributions from the walls separating the two containers, while at the fictitious boundaries of the domain, Maxwellians defined by the local pressure P_1 or P_2, temperature T_0 and zero bulk velocity are specified as the incoming distributions. Symmetry boundary conditions are imposed at $r = 0$. Based on the above, the boundary conditions in dimensionless form for the orifice flow are:

Upstream reservoir

$$g^+(-X_L/R, r, c_x, c_p, \theta) = g^+(x, Y_L/R, c_x, c_p, \theta) = \frac{1}{\pi^{3/2}} e^{-c^2} \tag{32}$$

Downstream reservoir

$$g^+(X_R/R, r, c_x, c_p, \theta) = g^+(x, Y_R/R, c_x, c_p, \theta) = \frac{P_2}{P_1}\frac{1}{\pi^{3/2}} e^{-c^2} \tag{33}$$

Partition wall

$$g^+(x \to 0^{\mp}, r, c_x, c_p, \theta) = \frac{\rho_{\mp}^{\text{orifice}}}{\pi^{3/2}} e^{-c^2} \tag{34}$$

In all cases the superscripts $(+)$ denotes outgoing distributions, while the notation $(\mp)$ denotes the left $(-)$ and right $(+)$ sides of the partition wall. Finally, in Eq. (34) the quantities $\rho_{\mp}$ are specified by the no penetration condition at each side

$$\rho_{-}^{\text{orifice}} = 4\sqrt{\pi} \int_0^{\infty}\int_0^{\pi}\int_0^{\infty} c_x g\left(0^-, r, c_x, c_p, \theta\right) c_p dc_p d\theta dc_x \tag{35}$$

$$\rho_{+}^{\text{orifice}} = -4\sqrt{\pi} \int_{-\infty}^{0}\int_0^{\pi}\int_0^{\infty} c_x g\left(0^+, r, c_x, c_p, \theta\right) c_p dc_p d\theta dc_x \tag{36}$$

Summarizing the formulation it is noted that the flow through a slit is described by the kinetic equations (5,6) coupled by the moments (9–12) and subject to boundary conditions (16–21), while the parameters $\rho_{\mp}^{\text{slit}}$ are given by (22,23). The flow through an orifice is described by kinetic equation (24) coupled by the moments (25–28) and subject to boundary conditions (32–34), while the parameters $\rho_{\mp}^{\text{orifice}}$ are given by (35,36). The solution of the two problems depends on two dimensionless parameters, namely the reference rarefaction parameter δ_0 and the pressure ratio P_2/P_1.

Table 1
Dimensionless flow rate through a slit W vs. rarefaction parameter and pressure ratio.

W_{slit}					
	$P_2/P_1 = 0$		$P_2/P_1 = 0.5$		$P_2/P_1 = 0.9$
δ_0	BGK	DSMC [6]	BGK	DSMC [7]	BGK
0	1.000	–	0.500	–	0.100
0.01	1.003	1.001	0.502	–	0.101
0.1	1.025	1.017	0.519	0.520	0.105
1	1.162	1.139	0.651	0.640	0.138
5	1.383	1.373	1.031	1.015	0.260
10	1.474	1.479	1.238	1.237	0.391
100	1.549	1.566	1.372	1.383	0.678

4. Numerical scheme

The kinetic equations for both problems under consideration are discretized in the molecular velocity and physical spaces. In particular, the continuum spectrum of the components c_x and c_p of the molecular velocity vector is replaced by a set of discrete magnitudes $c_x^m \in [0, c_x^{\max}]$ and $c_p^m \in [0, c_p^{\max}]$, with m = 1,2,…,$M$, which are taken to be the roots of the Legendre polynomial of order M accordingly mapped from $[-1,1]$ to $[0, c_{x,p}^{\max}]$. Also, the polar angle space is discretized in θ_k, k = 1,2,…,K angles, uniformly distributed in $[0,2\pi]$ for the Cartesian geometry and by making use of the axisymmetry in $[0,\pi]$ in the Cylindrical geometry. In the physical space the computational domain is discretized using $(I \times J)$ square elements of side h. At each square element (i,j), i = 1,2,…,I and j = 1,2,…J a central second-order scheme in space is applied. In addition, the macroscopic moments of the reduced distributions are estimated by double or triple numerical integration consisting of one or two Gauss-Legendre quadratures and the trapezoidal rule. A similar approach has been implemented in Ref. [14,15].

Then, the discretized equations are solved in an iterative manner consisting of two steps. In the first step, the kinetic equations are solved for the unknown distributions assuming that the macroscopic quantities at the right hand side of the kinetic equations are known. In the second step, updated estimates of the macroscopic quantities are computed based on the moments of the distribution functions. The iterative procedure is ended when the termination criterion is satisfied. This is the typical iteration scheme used in discrete velocity kinetic solvers. However, due to the fact that the regions at the inlet and at the outlet of the computational domain must be adequately large, the computational cost rises significantly.

Therefore, here this typical algorithm has been upgraded by making use of a) message passing interface (MPICH2), b) memory handling techniques and c) automated grid refinement. The parallelization of the kinetic algorithm is implemented in the

Table 2
Dimensionless flow rate through an orifice W vs. rarefaction parameter and pressure ratio.

W_{orifice}						
	$P_2/P_1 = 0$		$P_2/P_1 = 0.5$		$P_2/P_1 = 0.9$	
δ_0	BGK	DSMC [8]	BGK	DSMC [8]	BGK	DSMC [8]
0	1.000	–	0.500	–	0.100	–
0.01	1.002	–	0.502	–	0.101	–
0.1	1.020	1.014	0.515	0.509	0.105	0.103
1	1.152	1.129	0.635	0.613	0.140	0.130
5	1.387	–	1.029	–	0.280	–
10	1.472	1.462	1.216	1.188	0.432	0.402
100	1.508	1.534	1.325	1.344	0.669	0.674

molecular velocity space. This is a simple and natural way of parallelization inherent in the structure of the algorithm reducing significantly the required computational effort. The estimates of the distribution functions at each processor are summed to estimate the updated macroscopic quantities. Before starting a new iteration, the macroscopic quantities and the impermeability constants are synchronized and re-transmitted to each processor. This procedure takes place in the host computer of the parallel scheme. The computational effort during the first step of the iteration, which is the most computationally demanding, can be split up to $M \times K$ processors, which correspond to the total number of discrete velocities, for the case of the slit and M^2 processors for the case of the orifice. The scaling characteristics of the algorithm are quite good, considering the number of variables that must be exchanged at each iteration. An average efficiency of about 94% for 64 processors and 75% for 256 processors is calculated. It is expected that extending the parallelization in the physical space will further reduce the computational cost.

Furthermore, memory handling techniques have been used to reduce storage requirements due to the 4D and 5D of the distribution function for the slit and orifice flows respectively. Due to the velocity magnitude independency, a temporary array can be allocated and overwritten after treating each magnitude. The dimensionality of this array can be further reduced by storing the distribution only in the parts of the domain required by the marching scheme of the discretized governing equation. For

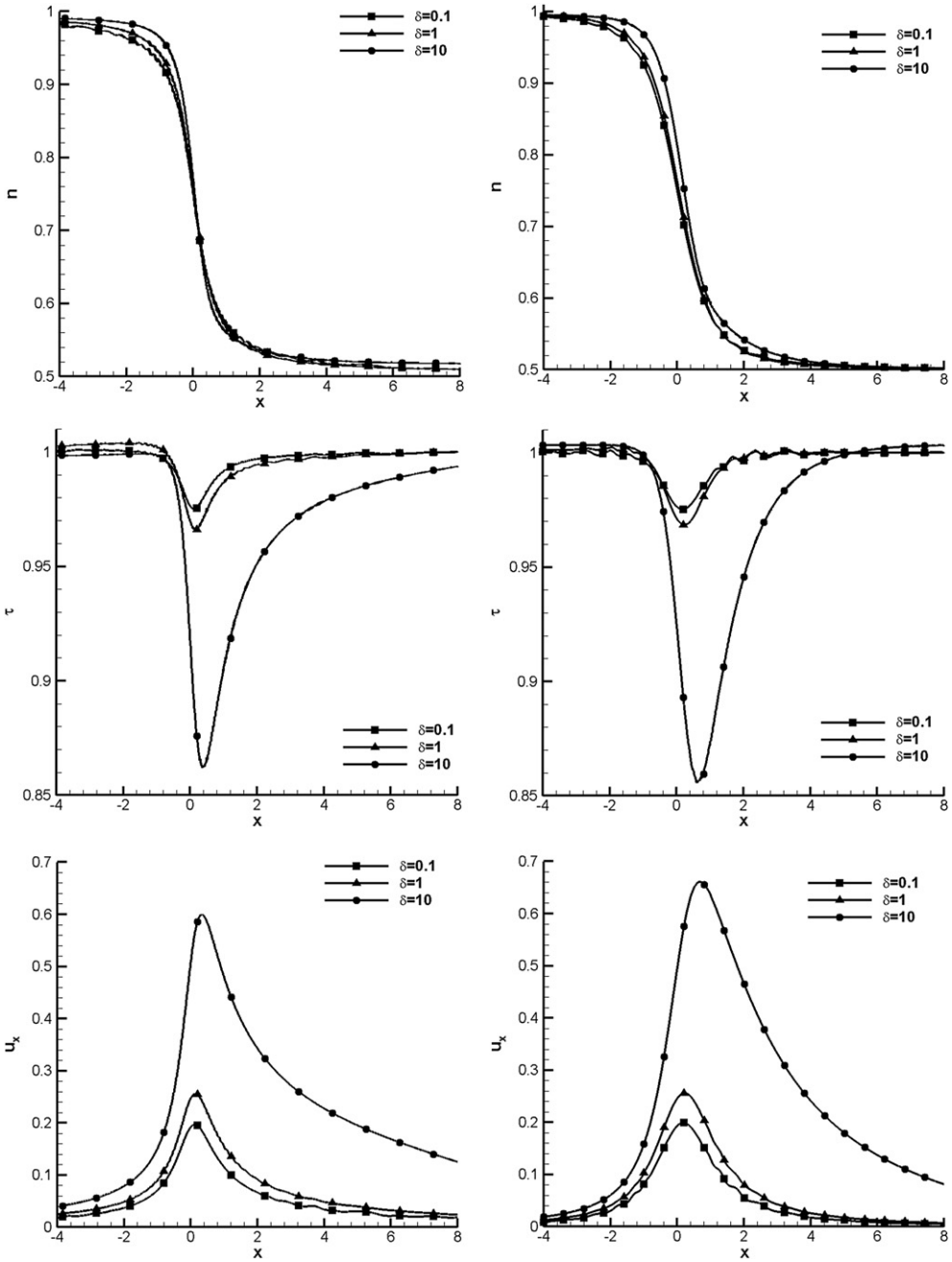

Fig. 2. Distributions of number density (top), temperature (middle) and axial velocity (bottom) along the symmetry axis for flow through a slit (left) and an orifice (right) with $P_2/P_1 = 0.5$ and $\delta_0 = 0.1$, 1 and 10.

example, for the marching procedure toward the positive x -direction, the distribution is stored only at positions x and $x - \Delta x$. These techniques permit having a two-dimensional array for the distribution function and practically remove memory limitations. In this manner, channels of any length can be considered, since the size of this array is only determined by the height of the entrance/exit regions and the number of angles in the case of the orifice.

Finally, grid refinement techniques have been implemented in order to accelerate the convergence of the numerical scheme. In this context, the simulations are initially performed with a smaller amount of nodes. After convergence has been reached, the simulation procedure is repeated in a refined mesh, where the physical space parameters have been doubled, using the previous solution as an initial condition. Linear interpolation has been used here as a first approximation. This procedure is repeated until the final number of nodes has been reached. Following this multiple grid procedure, the gain in the number of iterations for large values of δ_0 is significant. It is noted that the number of iterations in dense grids is about two orders of magnitude smaller than the corresponding one in sparse grids and therefore the overall CPU time is greatly reduced.

5. Results and discussion

Numerical results are presented in dimensionless form for the flow rates and the macroscopic distributions for the slit and orifice flows in a wide range of the rarefaction parameter $\delta_0 \in [0,100]$ and three pressure ratios $P_2/P_1 = 0$, 0.5 and 0.9. The presented results have been obtained with the upstream and downstream computational domains varying from 20×8 up to 40×15 depending on the pressure ratio and rarefaction parameter. The iteration process is terminated when a relative convergence criterion of 10^{-6} imposed on the average residual of each computed macroscopic quantity per node is fulfilled. Regarding the accuracy of the presented results, it is noted that all numerical parameters (number of nodes in the physical space, magnitudes and angles in the molecular velocity space, size of inlet and outlet regions, convergence criterion) have been modified in order to ensure that the presented results are grid independent up to at least two significant figures. This accuracy requires CPU time of hours ($\delta_0 \leq 1$), days ($\delta_0 = 10$) and weeks ($\delta_0 = 100$).

The dimensionless flow rates W through a slit and an orifice are tabulated in Tables 1 and 2, respectively. In both cases the flow rate is monotonically increased as the rarefaction parameter δ_0 is increased. It is seen that the increase of W is small in the free molecular and continuum regimes and more rapid in the transition regime. Also, in both cases W is decreased as the pressure ratio P_2/P_1 is increased (i.e., the pressure difference between the two reservoirs becomes smaller). It is also seen that as P_2/P_1 is increased the dependency of W on δ_0 becomes weaker.

For comparison purposes, corresponding results available in the literature for the slit [6,7] and the orifice [8] flow problems obtained by the DSMC method are included in Tables 1 and 2 respectively. It is seen that for $P_2/P_1 = 0$ and 0.5 the BGK and DSMC results agree up to at least two significant figures. This very good agreement clearly demonstrates the accuracy of the kinetic algorithm and furthermore the reliability of the BGK model for simulating pressure driven flows. For $P_2/P_1 = 0.9$ available DSMC results exist only for the orifice flow. In this case the agreement remains very good up to $\delta_0 = 1$ and then at $\delta_0 = 10$ and 100 is reduced but always remains within 7%. It is important to note that, for both the BGK and DSMC algorithms, the required computational effort is increased as δ_0 is increased. However, as the pressure ratio P_2/P_1 is increased the required computational effort for the DSMC algorithm is increased, while this is not the case for the kinetic algorithm, the computational effort of which is slightly reduced as the pressure ratio is increased. This is a significant advantage of the kinetic compared to the DSMC approach.

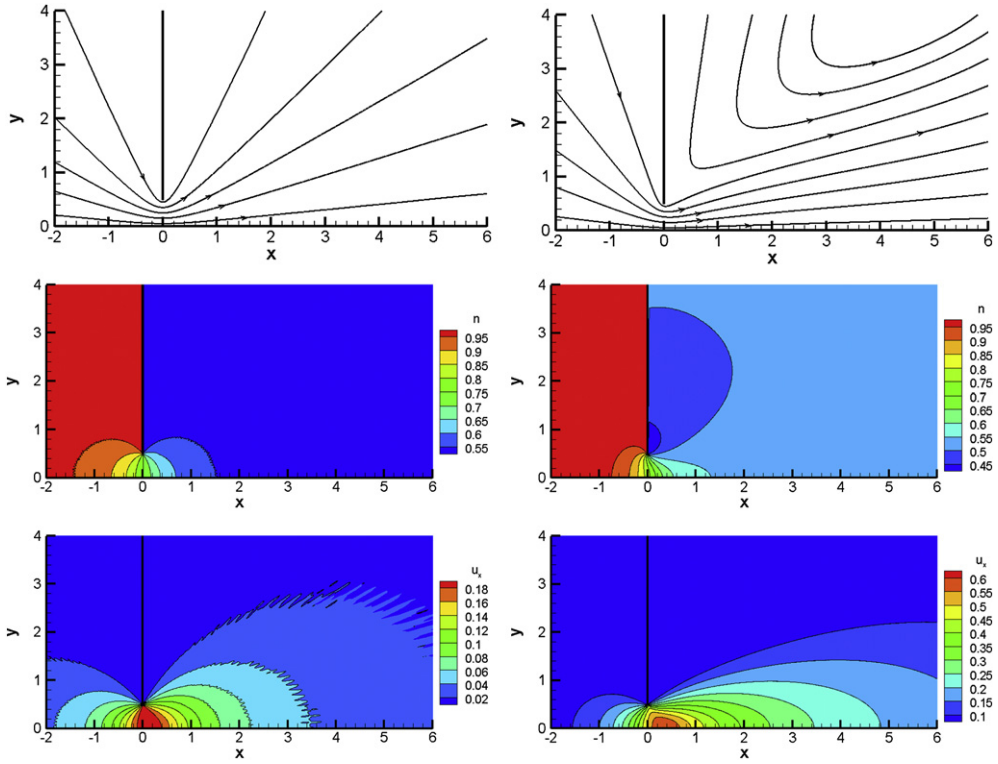

Fig. 3. Flow through a slit for $P_2/P_1 = 0.5$ and $\delta_0 = 0.1$ (left) and 10 (right); streamlines (top) and isolines of number density (middle) and axial velocity (bottom).

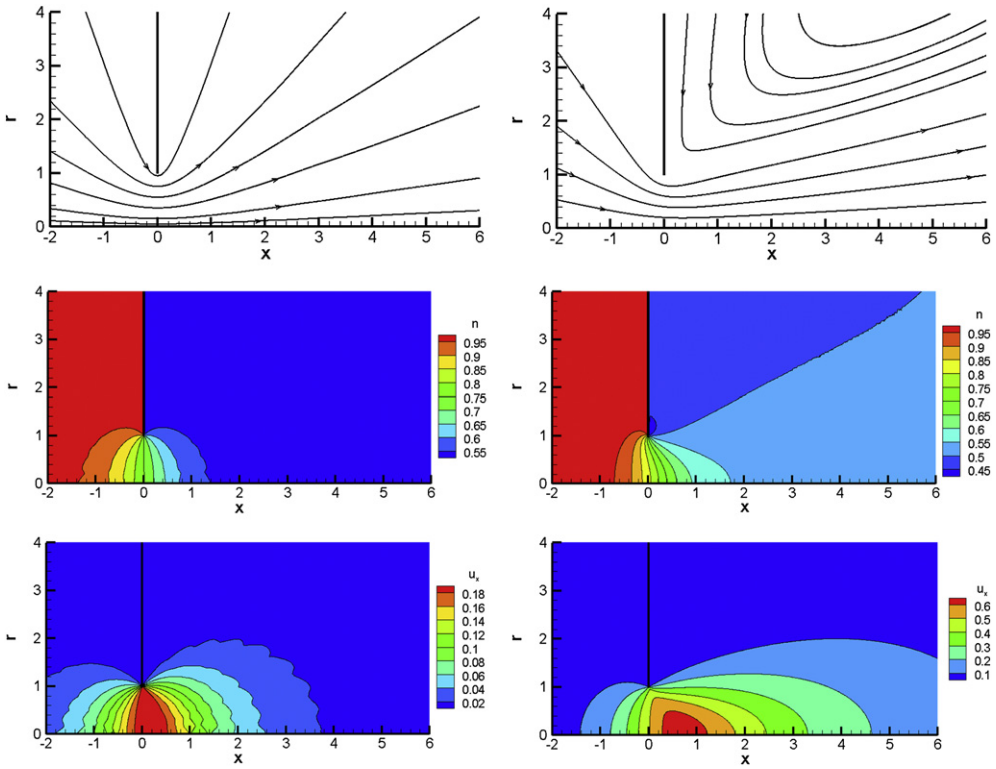

Fig. 4. Flow through an orifice for $P_2/P_1 = 0.5$ and $\delta_0 = 0.1$ (left) and 10 (right); streamlines (top) and isolines of number density (middle) and axial velocity (bottom).

Macroscopic distributions and typical pictures of the flow field are shown in Figs. 2–4. In Fig. 2, the dimensionless number density, temperature and axial velocity, for both a slit and an orifice flow, along the symmetry axis is shown for three characteristic values of the rarefaction parameter and $P_2/P_1 = 0.5$. It is seen that the variation of the corresponding macroscopic quantities in the slit and orifice flow is qualitatively similar. Starting with the density variation, it is seen that far upstream is equal to one, it is rapidly decreased in the region one unit length before and after the wall partition and then it gradually approaches the far downstream conditions. The temperature equals unity in most of the domain, while close to the partition it is decreased. The drop is related to the rarefaction parameter and ranges from around 4% for small values of δ_0 up to about 16% for $\delta_0 = 10$. The axial velocity far upstream is almost zero and is increased in the region just before the partition, while after the partition it is decreased to almost zero far downstream. The maximum value of the velocity is increased as δ_0 is increased. The above described behavior is typical for the corresponding macroscopic quantities when $P_2/P_1 \neq 0$.

In Figs. 3 and 4, a more complete picture of the flow fields is provided for the slit and orifice geometries respectively. Flow streamlines along with isolines of number density and axial velocity are plotted for $P_2/P_1 = 0.5$ and $\delta_0 = 0.1$ and 10. Again, there is a qualitative resemblance between the corresponding slit and the orifice flows. It is seen that the structure of the flow field between rarefied and dense atmospheres is different. At $\delta_0 = 0.1$ the streamlines are almost symmetric with regard to the y axis, while at $\delta_0 = 10$ there is no symmetry and a vortex appears next to the partition at the downstream container. Also, as the atmosphere becomes more dense, the flow accelerates faster and the maximum axial velocity is increased. The saw-like shape of the isolines appearing for the small values of the rarefaction parameter has only numerical character and it is not related to the physical properties of the flow. This is a disadvantage of the discrete velocity method which is not easily circumvented.

6. Concluding remarks

An efficient fully deterministic kinetic algorithm has been applied for the solution of the pressure driven slit and orifice flows. By solving the BGK kinetic model subject to Maxwell boundary conditions the flow rates and the macroscopic quantities of the flows have been obtained. The computational algorithm includes parallelization in the molecular velocity space, drastic reduction in memory demands and acceleration of the iteration map by multiple grid methods. The results are in very good agreement with previously reported DSMC results, clearly indicating the accuracy of the proposed algorithm and the reliability of the BGK model for solving pressure driven flows.

Acknowledgments

This work has been supported by the European Communities under the contract of Association EURATOM/Hellenic Republic. The views and opinions expressed herein do not necessarily reflect those of the European Commission.

References

[1] Sharipov F. Rarefied gas flow through a long rectangular channel. J Vac Sci Technol A 1999;17:3062–6.
[2] Naris S, Valougeorgis D. Rarefied gas flow in a triangular duct based on a boundary fitted lattice. Eur J Mech B/Fluids 2008;27:810–22.
[3] Varoutis S, Naris S, Hauer V, Day C, Valougeorgis D. Computational and experimental study of gas flows through long channels of various cross sections in the whole range of the Knudsen number. J Vac Sci Technol A 2009; 27:89–100.
[4] Naris S, Valougeorgis D, Kalempa D, Sharipov F. Flow of gaseous mixtures through rectangular microchannels driven by pressure, temperature, and concentration gradients. Phys Fluids 2005;17:100607.1–100607.12.
[5] Bird GA. Molecular gas dynamics and the direct simulation of gas flows. Oxford: Oxford University Press; 1994.

[6] Sharipov F, Kozak D. Rarefied gas flow through a thin slit into vacuum simulated by the Monte Carlo method over the whole range of the Knudsen number. J Vac Sci Technol A 2009;27:479–84.
[7] Sharipov F, Kozak D. Rarefied gas flow through a thin slit at an arbitrary pressure ratio. Eur J Mech B/Fluids 2011;30:543–9.
[8] Sharipov F. Numerical simulation of rarefied gas flow through a thin orifice. J Fluid Mech 2009;518:35–60.
[9] Varoutis S, Valougeorgis D, Sazhin O, Sharipov F. Rarefied gas flow through short tubes into vacuum. J Vac Sci Technol A 2008;26:228–38.
[10] Varoutis S, Valougeorgis D, Sharipov F. Simulation of gas flow through tubes of finite length over the whole range of rarefaction for various pressure drop ratios. J Vac Sci Technol A 2009;27:1377–91.
[11] Chigullapalli S, Venkattraman A, Ivanov MS, Alexeenko AA. Entropy considerations in numerical simulations of non-equilibrium rarefied flows. J Comp Phys 2010;229:2139–58.
[12] Gimelshein N, Gimelshein S, Selden N, Ketsdever A. Modeling of low-speed rarefied gas flows using a combined ES-BGK/DSMC approach. Vacuum 2010; 85:115–9.
[13] Titarev V, Shakhov E. High-order accurate conservative method for computing the poiseuille rarefied gas flow in a channel of arbitrary cross section. Comp Math Math Phys 2010;50:537–48.
[14] Pantazis S, Valougeorgis D. Heat transfer through rarefied gases between coaxial cylindrical surfaces with arbitrary temperature difference. Eur J Mechanics B/Fluids 2010;29:494–509.
[15] Pantazis S. Simulation of transport phenomena in conditions far from thermodynamic equilibrium via kinetic theory with applications in vacuum technology and MEMS. Ph.D. thesis: University of Thessaly. Volos, Greece; 2011.
[16] Graur IA, Polykarpov A Ph, . Sharipov F. Numerical modelling of rarefied gas flow through a slit into vacuum based on the kinetic equation. Comput Fluids 2011;49:87–92.
[17] Graur A, Polykarpov A Ph, Sharipov F. Numerical modelling of rarefied gas flow through a slit at arbitrary gas pressure ratio based on the kinetic equation. Z Angew Math Phys 2011;49:1–18.
[18] Sharipov F, Kremer GM. On the frame dependence of constitutive equations. i. Heat transfer through a rarefied gas between two rotating cylinders. Continuum Mech Thermodyn 1995;7:57–71.